Engineering Fracture Mechanics Vol. 32, No. 2, pp. 265–278, 1989
Printed in Great Britain.

0013-7944/89 $3.00 + .00

POST-PEAK AND POST-BIFURCATION ANALYSIS OF COHESIVE CRACK PROPAGATION

ALBERTO CARPINTERI
Department of Structural Engineering, Politecnico di Torino, 10129 Torino, Italy

Abstract—A cohesive crack model is applied to analyse the crack stability in elastic-softening materials. The shape of the global load–displacement response changes substantially by varying size-scale and keeping geometrical shape of the structure unchanged. The softening branch becomes steeper and steeper when the size-scale increases. A critical size-scale does exist for which the softening slope is infinite. In such a case, the load carrying capacity drastically decreases for relatively small displacement increments. Then, for larger size-scales, the softening slope becomes positive and a cusp catastrophe appears. It is proved that such a bifurcation point can be revealed by the simple *LEFM* condition $K_I = K_{IC}$.

1. INTRODUCTION

THE PROBLEM of transferability of small specimen data to full-size scale structural components is faced. Due to the different physical dimensions of tensile strength and fracture toughness, size-scale effects are always present in material testing. For the specimen sizes normally used, plastic flow or ultimate strength collapse at the ligament tends to anticipate the true propagation of the initial crack. On the other hand, whereas in classical solid mechanics only energy dissipation per unit of volume is considered (e.g. Von Mises equivalent stress), in fracture mechanics energy dissipation per unit of area is also involved (e.g. strain energy release rate). The co-existence of the two local collapse mechanisms (plasticity and fracture) can then produce peculiar size effects on the global structure behaviour.

Two fundamental questions arise dramatically.

(1) Are the data coming from small-scale specimens related to the collapse conditions in large-scale structures?
(2) If the ductile fracture in small-scale specimens is not completely obscured by the plastic flow collapse at the ligament, how is it possible to put the former in connection with the brittle fracture in large-scale structures?

The competition between collapses of a different nature can be emphasized with the application of dimensional analysis and considering the maximum loads derived from LEFM and limit analysis respectively. The transition from ductile to brittle behaviour is governed by a non-dimensional brittleness number, which is a function of material properties and structure size-scale. A true LEFM collapse occurs only with relatively low fracture toughnesses and/or large structure sizes [1–3].

A cohesive crack model is applied to analyse the local or slow crack growth in elastic-softening materials. The shape of the global load–displacement response changes substantially by varying size-scale and keeping geometrical shape of the structure unchanged. The softening branch becomes steeper and steeper when the size-scale increases. A critical size-scale does exist for which the softening slope is infinite. In such a case the load carrying capacity drastically decreases for relatively small displacement increments. Then, for size-scales larger than the critical one, the softening slope becomes positive and part of the load–displacement path proves to be virtual if the loading process is displacement-controlled. In such a case, the loading capacity will present a discontinuity with a negative jump. The size-scale transition from ductile to brittle behaviour is governed by the non-dimensional brittleness number, s_E. A truly brittle fracture occurs only with relatively low fracture toughnesses, $\mathcal{G}_{IC}$, high tensile strengths, σ_u, and/or large structure size-scales, b, i.e. when $s_E = \mathcal{G}_{IC}/\sigma_u b \to 0$.

On the other hand, if the loading process is controlled by a monotonically increasing function of time (e.g. the crack mouth opening displacement), the indentation in the load–displacement

curve can be captured experimentally [4]. When the post-peak behaviour is kept under control up to the complete structure separation, the area delimited by load–displacement curve and displacement-axis represents the product of $\mathcal{G}_{IC}$ by the initial ligament area.

Eventually, it is proved that, for $s_E \to 0$, the maximum load of catastrophical failure may be provided by the simple LEFM condition: $K_I = K_{IC} = \sqrt{(\mathcal{G}_{IC} E)}$ (plane stress), and that slow crack growth and process zone are lacking before the catastrophical event (snap-back).

2. APPLICATION OF DIMENSIONAL ANALYSIS

Due to the different physical dimensions of ultimate tensile strength, σ_u, and fracture toughness, K_{IC}, scale effects are always present in the usual fracture testing of common engineering materials. This means that, for the usual size-scale of the laboratory specimens, the ultimate strength collapse or the plastic collapse at the ligament tends to anticipate and obscure the brittle crack propagation. Such a competition between collapses of a different nature can easily be shown by considering the ASTM formula [5] for the three point bending test evaluation of fracture toughness (Fig. 1):

$$K_I = \frac{Pl}{tb^{3/2}} f\left(\frac{a}{b}\right), \tag{1}$$

with

$$f\left(\frac{a}{b}\right) = 2.9\left(\frac{a}{b}\right)^{1/2} - 4.6\left(\frac{a}{b}\right)^{3/2} + 21.8\left(\frac{a}{b}\right)^{5/2} - 37.6\left(\frac{a}{b}\right)^{7/2} + 38.7\left(\frac{a}{b}\right)^{9/2}.$$

At the crack propagation eq. (1) becomes:

$$K_{IC} = \frac{P_{max} l}{tb^{3/2}} f\left(\frac{a}{b}\right), \tag{2}$$

where P_{max} is the external load of brittle fracture.

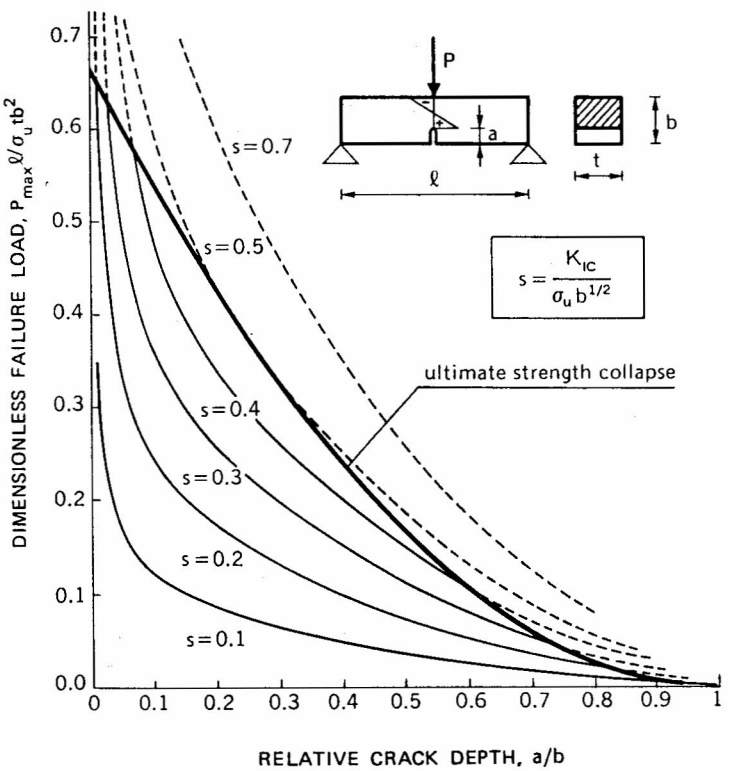

Fig. 1. Dimensionless load of crack instability vs relative crack depth.

If both members of eq. (2) are divided by $\sigma_u b^{1/2}$ we obtain:

$$\frac{K_{IC}}{\sigma_u b^{1/2}} = s = \frac{P_{max} l}{\sigma_u t b^2} f\left(\frac{a}{b}\right), \tag{3}$$

where s is a dimensionless number able to describe the brittleness of the specimen [1–3]. Rearranging eq. (3) gives:

$$\frac{P_{max} l}{\sigma_u t b^2} = \frac{s}{f\left(\frac{a}{b}\right)}. \tag{4}$$

On the other hand, it is possible to consider the non-dimensional load of ultimate strength in a beam of depth $(b - a)$:

$$\frac{P_{max} l}{\sigma_u t b^2} = \frac{2}{3}\left(1 - \frac{a}{b}\right)^2. \tag{5}$$

Equations (4) and (5) are plotted in Fig. 1 as functions of the crack depth a/b. While the former produces a set of curves by varying the brittleness number, s, the latter is represented by a unique curve. It is evident that the ultimate strength collapse at the ligament precedes crack propagation for each initial crack depth, when the brittleness number, s, is higher than the limit-value $s_0 = 0.50$.

For lower s numbers ultimate strength collapse anticipates crack propagation only for crack depths external to a certain interval. This means that a true LEFM collapse occurs only for comparatively low fracture toughnesses, high tensile strengths and/or large structure sizes. The single values of K_{IC}, σ_u and b do not determine the nature of the collapse, but rather their function, s (eq. 3).

3. VIRTUAL PROPAGATION OF A BRITTLE FRACTURE

The flexural behaviour of the beam in Fig. 1 will be analysed. The deflection due to the elastic compliance of the uncracked beam is:

$$\delta_e = \frac{P l^3}{48 E I}, \tag{6}$$

where I is the inertial moment of the cross-section with respect to the barycentric axis. On the other hand, the deflection due to the local crack compliance is [6]:

$$\delta_c = \frac{3}{2}\frac{P l^2}{t b^2 E} g\left(\frac{a}{b}\right), \tag{7}$$

with:

$$g\left(\frac{a}{b}\right) = \left(\frac{a/b}{1 - \frac{a}{b}}\right)^2 \left\{5.58 - 19.57\left(\frac{a}{b}\right) + 36.82\left(\frac{a}{b}\right)^2 - 34.94\left(\frac{a}{b}\right)^3 + 12.77\left(\frac{a}{b}\right)^4\right\}. \tag{8}$$

The superposition principle provides:

$$\delta = \delta_e + \delta_c,$$

and, in non-dimensional form:

$$\frac{\delta l}{\epsilon_u b^2} = \frac{P l}{\sigma_u t b^2}\left[\frac{1}{4}\left(\frac{l}{b}\right)^3 + \frac{3}{2}\left(\frac{l}{b}\right)^2 g\left(\frac{a}{b}\right)\right], \tag{9}$$

being $\epsilon_u = \sigma_u / E$. The term within square brackets is the dimensionless compliance, which results to be a function of the beam slenderness, l/b, as well as of the crack depth, a/b. Some linear load–deflection diagrams are represented in Fig. 2, by varying the crack depth a/b and for the fixed ratio $l/b = 4$.

Through eqs (4) and (5), it is possible to determine the point of crack propagation, as well as the point of ultimate strength on each linear plot in Fig. 2. Whereas the former depends on the

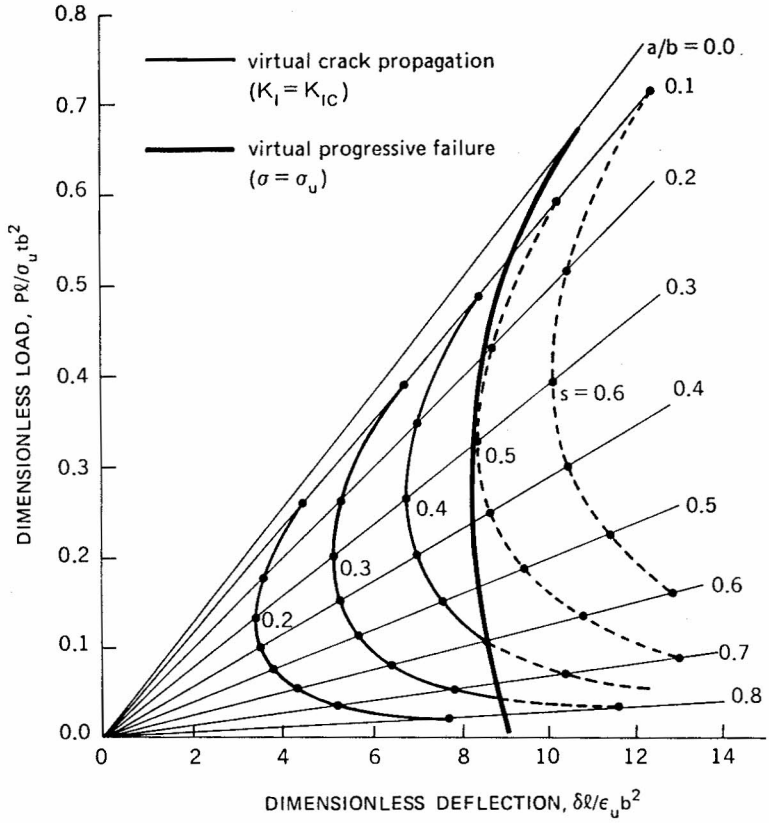

Fig. 2. Dimensionless load of crack instability vs dimensionless deflection.

brittleness number, s, the latter is unique. The set of the crack propagation points with s = constant and by varying the crack depth, represents a virtual load–deflection path, where point by point the load is always that producing the crack instability [7]. When the crack grows, the load of instability decreases and the compliance increases, so that the product at the right member of eq. (9) may result to be either decreasing or increasing. The diagrams in Fig. 2 show the deflection decreasing (with the load) up to the crack depth $a/b \simeq 0.3$, and then increasing (in discordance with the load). Therefore, whereas for $a/b \gtrsim 0.3$, the $P - \delta$ curve presents the usual softening course with negative derivative for $a/b \lesssim 0.3$ it presents positive derivative. Such a branch could not be revealed by deflection-controlled testing and the representative point would jump from the positive to the negative branch with a behaviour discontinuity.

The set of the ultimate strength points, by varying the crack depth, is represented by the thick line in Fig. 2. Such a line intersects the virtual crack propagation curves with $s \leqslant s_0 = 0.50$, analogous to what is shown in Fig. 1, and presents a slight indentation with $\mathrm{d}P/\mathrm{d}\delta > 0$.

The crack mouth opening displacement, w_1, is a function of the specimen geometry and of the elastic modulus [6]:

$$w_1 = \frac{6\,Pla}{tb^2E} h\left(\frac{a}{b}\right), \tag{10}$$

with:

$$h\left(\frac{a}{b}\right) = 0.76 - 2.28\left(\frac{a}{b}\right) + 3.87\left(\frac{a}{b}\right)^2 - 2.04\left(\frac{a}{b}\right)^3 + \frac{0.66}{\left(1 - \frac{a}{b}\right)^2}. \tag{11}$$

In non-dimensional form eq. (10) becomes:

$$\frac{w_1 l}{\epsilon_u b^2} = \frac{Pl}{\sigma_u tb^2}\left[6\left(\frac{l}{b}\right)\left(\frac{a}{b}\right)h\left(\frac{a}{b}\right)\right]. \tag{12}$$

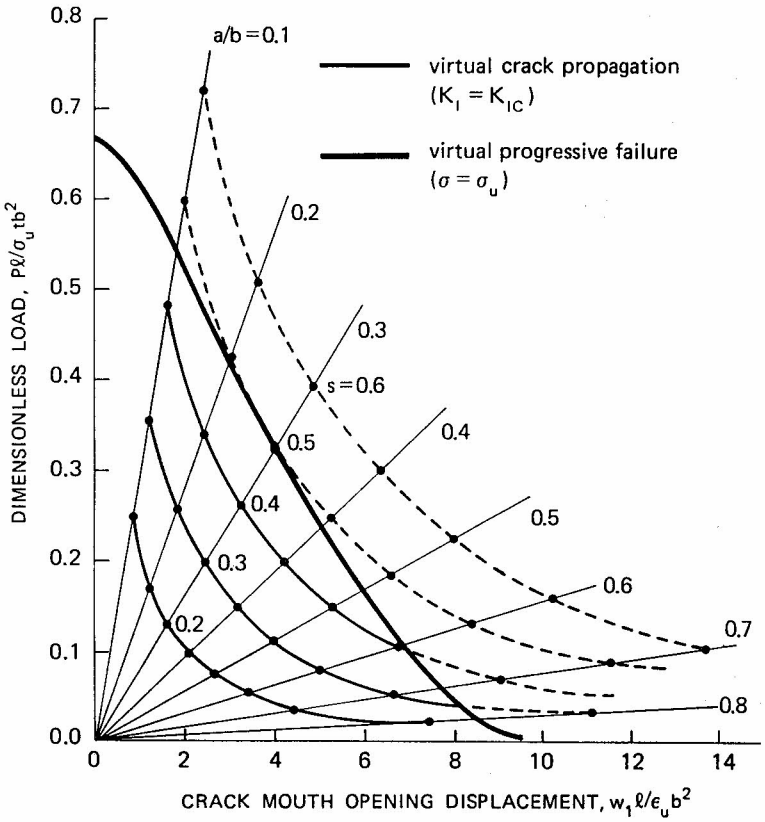

Fig. 3. Dimensionless load of crack instability vs dimensionless crack mouth opening displacement.

The term within square brackets is the dimensionless compliance which, also in this case, depends on beam slenderness and crack depth. Some linear load–crack mouth opening displacement diagrams are reported in Fig. 3, by varying the crack depth a/b and for $l/b = 4$.

The set of the crack propagation points with s = constant and by varying the crack depth, represents a virtual process even in this case. When the crack grows, the product at the right member of eq. (12) always increases, the compliance increase prevailing over the critical load decrease for each value of a/b. The P–w_1 curve always presents a negative derivative and the crack mouth opening displacement, w_1, increases even when load and deflection both decrease ($dP/d\delta > 0$) in the catastrophic P–δ diagram. If the crack mouth opening displacement is controlled, i.e. if w_1 increases monotonically without jumping, it would be possible to go along the virtual P–δ path with positive slope. Such a theoretical statement was confirmed experimentally in [4].

The set of the ultimate strength points, by varying the crack depth, is represented by the thick line in Fig. 3, which intersects the crack propagation curves with $s \leq s_0 = 0.50$ (see also Figs 1 and 2).

4. COHESIVE CRACK MODEL

The cohesive crack model is based on the following assumptions [8–12].

(1) The cohesive fracture zone (plastic or process zone) begins to develop when the maximum principal stress achieves the ultimate tensile strength σ_u (Fig. 4a).
(2) The material in the process zone is partially damaged but still able to transfer stress. Such a stress is dependent on the crack opening displacement, w (Fig. 4b).

The energy necessary to produce a unit crack surface is given by the area under the σ–w diagram in Fig. 4(b):

$$\mathcal{G}_{IC} = \int_0^{w_c} \sigma \, dw = \tfrac{1}{2}\sigma_u w_c.$$

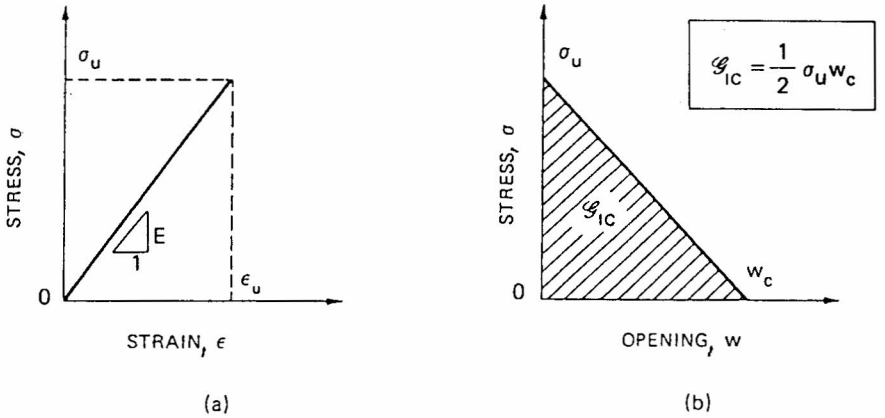

Fig. 4. Stress–strain (a) and stress–crack opening displacement (b) constitutive laws.

The real crack tip is defined as the point where the distance between the crack surfaces is equal to the critical value of crack opening displacement, w_c, and the normal stress vanishes (Fig. 5a). On the other hand, the fictitious crack tip is defined as the point where the normal stress attains the maximum value σ_u and the crack opening vanishes (Fig. 5a).

A three point bending slab of elastic-softening material is considered (Fig. 1). The displacement discontinuities on the center line may be expressed as follows:

$$w(x) = \int_0^b K(x, y)\sigma(y)\,dy + C(x)P + T(x), \quad \text{for} \quad 0 \leqslant x < b, \tag{13}$$

where K and C are the influence functions of cohesive forces and external load respectively, and T are the crack openings due to the specimen weight. If a stress-free crack of length a has developed with a cohesive zone of length Δa, the following additonal conditions are to be taken into account:

$$\sigma(y) = 0, \quad \text{for} \quad 0 \leqslant y \leqslant a, \tag{14a}$$

$$\sigma(y) = \sigma_u\left[1 - \frac{w(y)}{w_c}\right], \quad \text{for} \quad a \leqslant y \leqslant (a + \Delta a), \tag{14b}$$

$$w(x) = 0, \quad \text{for} \quad (a + \Delta a) \leqslant x < b. \tag{14c}$$

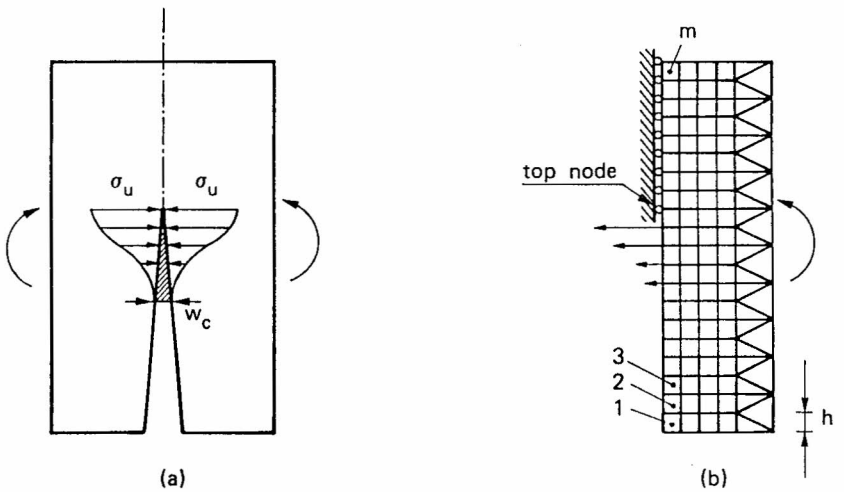

Fig. 5. Stress distribution across the cohesive zone (a) and equivalent nodal forces in the finite element mesh (b).

Equations (13) and (14) can be rearranged as follows:

$$w(x) = \int_a^{a+\Delta a} K(x,y)\left[1 - \frac{w(y)}{w_c}\right]\sigma_u \, dy + \int_{a+\Delta a}^{b} K(x,y)\sigma(y)\, dy + C(x)P + T(x),$$

$$\text{for} \quad 0 \leqslant x \leqslant (a + \Delta a), \tag{15a}$$

$$w(x) = 0, \quad \text{for} \quad (a + \Delta a) \leqslant x < b. \tag{15b}$$

The function $\sigma(y)$ depends on the distribution $w(x)$ and on the external load P. Therefore, for each value of P, eq. (15a) represents an integral equation for the unknown function w. On the other hand, the beam deflection is given by:

$$\delta = \int_0^b C(y)\sigma(y)dy + D_p P + D_\gamma, \tag{16}$$

where D_p is the deflection for $P = 1$ and D_γ is the deflection due to the specimen weight.

A numerical procedure is implemented to simulate a loading process where the parameter incremented step by step is the fictitious crack depth. Real (or stress-free) crack depth, external load and deflection are obtained at each step after an iterative computation.

The closing stresses acting on the crack surfaces (Fig. 5a) are replaced by nodal forces (Fig. 5b). The intensity of those forces depends on the opening of the fictitious crack, w, according to the σ–w constitutive law of the material (Fig. 4b). When the tensile strength σ_u is achieved at the fictitious crack tip (Fig. 5b), the top node is opened and a cohesive force starts acting across the crack, while the fictitious crack tip moves to the next node.

With reference to the three point bending test (TPBT) geometry in Fig. 6, the nodes are distributed along the potential fracture line. The coefficients of influence in terms of node openings and deflection are computed by a finite element analysis where the fictitious structure in Fig. 6 is subjected to $(n + 1)$ different loading conditions. Consider the TPBT in Fig. 7(a) with the initial crack tip in the node k. The crack opening displacements at the n fracture nodes may be expressed as follows:

$$\mathbf{w} = \mathbf{K}\mathbf{F} + \mathbf{C}P + \mathbf{T}, \tag{17}$$

where

$\mathbf{w}$ = vector of the crack opening displacements,
$\mathbf{K}$ = matrix of the coefficients of influence (nodal forces),
$\mathbf{F}$ = vector of the nodal forces,
$\mathbf{C}$ = vector of the coefficients of influence (external load),
P = external load,
$\mathbf{T}$ = vector of the crack opening displacements due to the specimen weight.

On the other hand, the initial crack is stress-free and therefore:

$$F_i = 0, \quad \text{for} \quad i = 1, 2, \ldots, (k-1), \tag{18a}$$

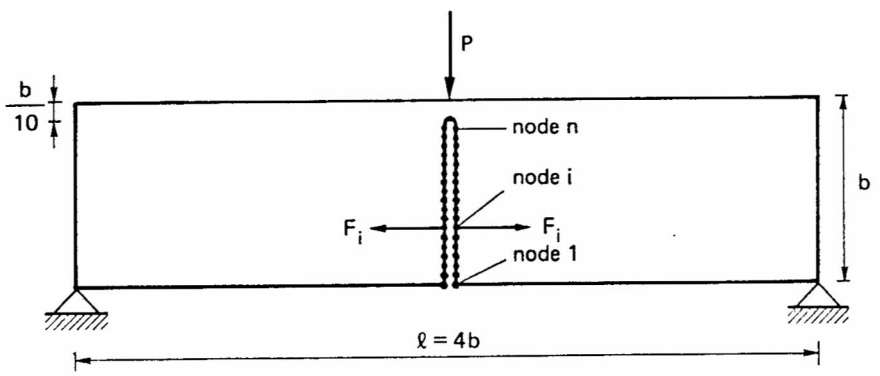

Fig. 6. Finite element nodes along the potential fracture line.

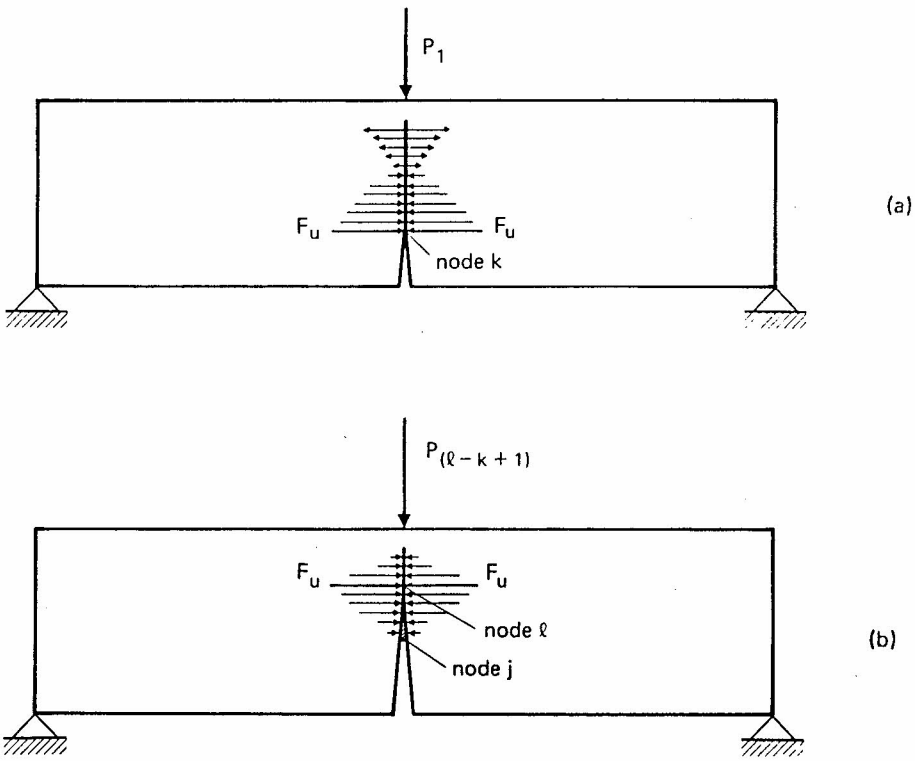

Fig. 7. Cohesive crack configurations at the first (a) and $(1-k+1)$th (b) crack growth increment.

while at the ligament there is no displacement discontinuity:

$$w_i = 0, \quad \text{for} \quad i = k, \quad (k+1), \ldots, n. \tag{18b}$$

Equations (17) and (18) constitute a linear algebraic system of $2n$ equations and $2n$ unknowns, i.e. the elements of vectors **w** and **F**. If load P and vector **F** are known, it is possible to compute the beam deflection, δ:

$$\delta = \mathbf{C}^T\mathbf{F} + D_P P + D_\gamma. \tag{19}$$

After the first step, a cohesive zone forms in front of the real crack tip (Fig. 7b), say between nodes j and l. Then eqs (18) are replaced by:

$$F_i = 0, \quad \text{for} \quad i = 1, 2, \ldots, (j-1), \tag{20a}$$

$$F_i = F_u\left(1 - \frac{w_i}{w_c}\right), \quad \text{for} \quad i = j, \quad (j+1), \ldots, l, \tag{20b}$$

$$w_i = 0, \quad \text{for} \quad i = l, \quad (l+1), \ldots, n, \tag{20c}$$

where F_u is the ultimate strength nodal force (Fig. 5*b*):

$$F_u = b\sigma_u/m. \tag{21}$$

Equations (17) and (20) constitute a linear algebraic system of $(2n+1)$ equations and $(2n+1)$ unknowns, i.e. the elements of vectors **w** and **F** and the external load P.

At the first step, the cohesive zone is missing ($l = j = k$) and the load P_1 producing the ultimate strength nodal force F_u at the initial crack tip (node k) is computed. Such a value P_1, together with the related deflection δ_1 computed through eq. (19), gives the first point of the $P - \delta$ curve. At the second step, the cohesive zone is between the nodes k and $(k+1)$, and the load P_2 producing the force F_u at the second fictitious crack tip (node $k+1$) is computed. Equation (19) then provides the deflection δ_2. At the third step, the fictitious crack tip is in the node $(k+2)$, and so on. The present numerical program simulates a loading process where the controlling parameter is the

fictitious crack depth. On the other hand, real (or stress-free) crack depth, external load and deflection are obtained at each step after an iterative procedure.

The program stops with the untying of the node n and, consequently, with the determination of the last couple of values F_n and δ_n. In this way, the complete load–deflection curve is automatically plotted by the computer.

5. FICTITIOUS FRACTURE TOUGHNESS OF INITIALLY CRACKED MEMBERS

Some dimensionless load–deflection diagrams obtained numerically for an initial crack depth $a_0/b = 0.1$ ($\epsilon_u = 0.87 \times 10^{-4}$, $l = 4b$, $t = b$, $\nu = 0.1$) are displayed in Fig. 8(a), by varying the non-dimensional number [10]:

$$s_E = \frac{\mathscr{G}_{IC}}{\sigma_u b} = \frac{w_c}{2b}. \tag{22}$$

The *energy brittleness number*, s_E, is connected with the *stress brittleness number*, s, defined in eq. (3). Recalling, in fact, that in the plane stress condition:

$$\mathscr{G}_{IC} = K_{IC}^2/E, \tag{23}$$

eq. (22) gives:

$$s_E = s^2 \epsilon_u. \tag{24}$$

Also in this case, the specimen is brittle for low s_E numbers, i.e. for low fracture toughnesses, $\mathscr{G}_{IC}$, high tensile strengths, σ_u, and large sizes, b. For $s_E \lesssim 8.36 \times 10^{-5}$, the P–δ curve presents a softening part with positive slope and a catastrophical event (snap-back) occurs if the loading process is deflection-controlled.

The deeper the initial crack is, the more ductile the specimen behaviour results to be. This is confirmed in Fig. 8(b) and (c) where the initial crack depth is assumed to be 0.3 and 0.5 respectively.

The maximum loading capacity $P_{max}^{(I)}$ of initially cracked specimens, according to the cohesive crack model, is obtained from the $P-\delta$ diagrams in Fig. 8(a)–(c). On the other hand, the maximum

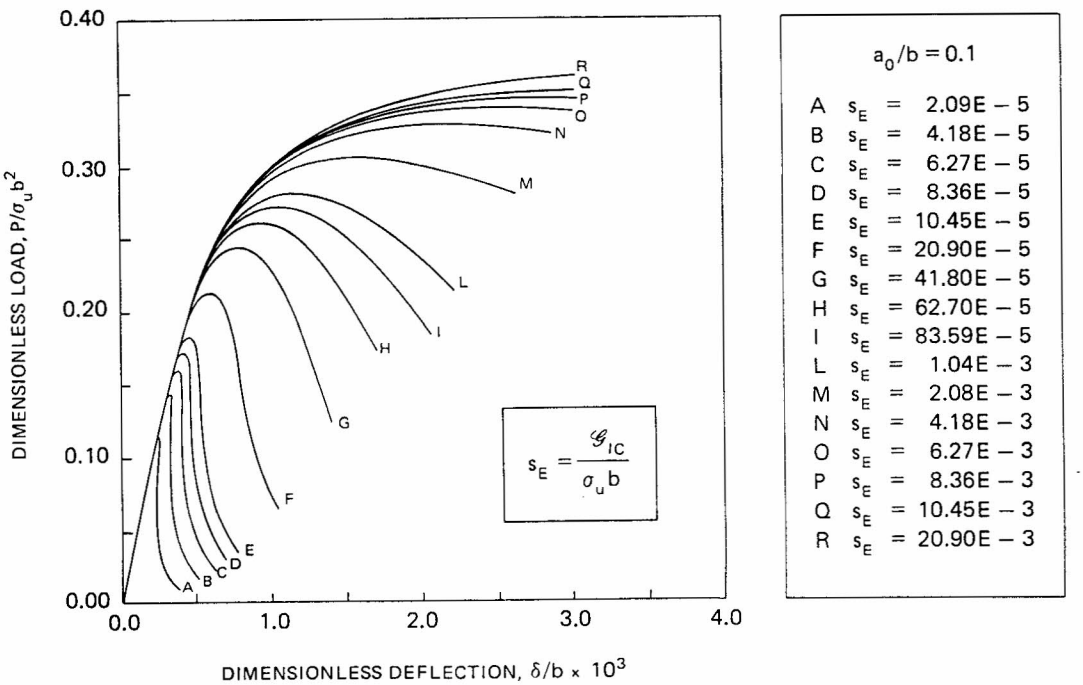

Fig. 8(a)

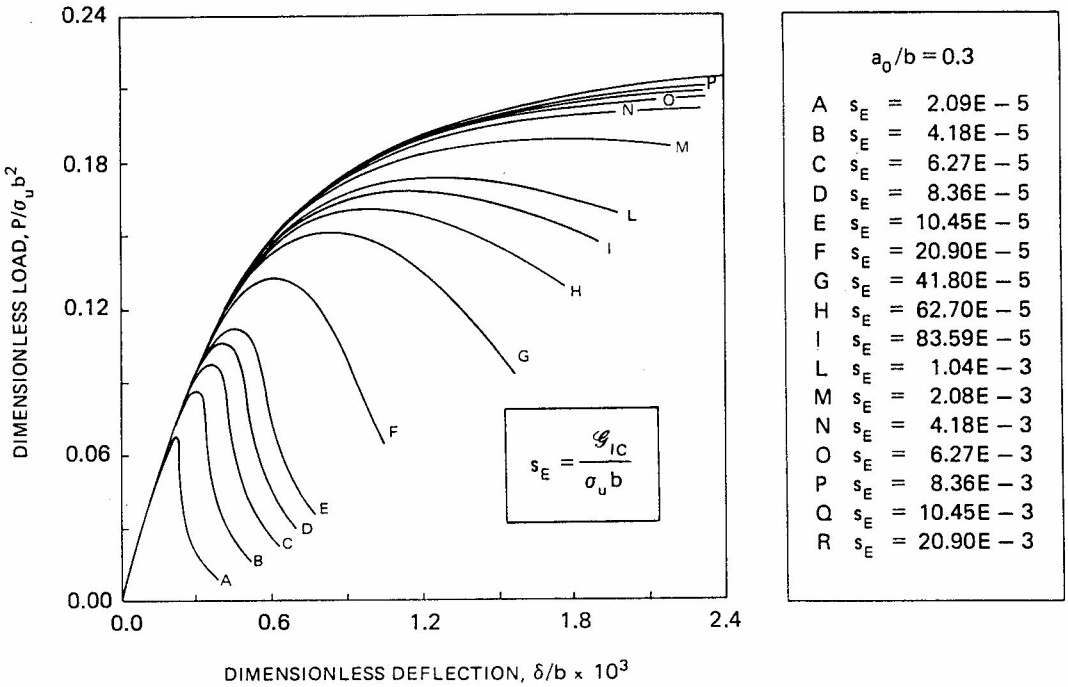

Fig. 8(b)

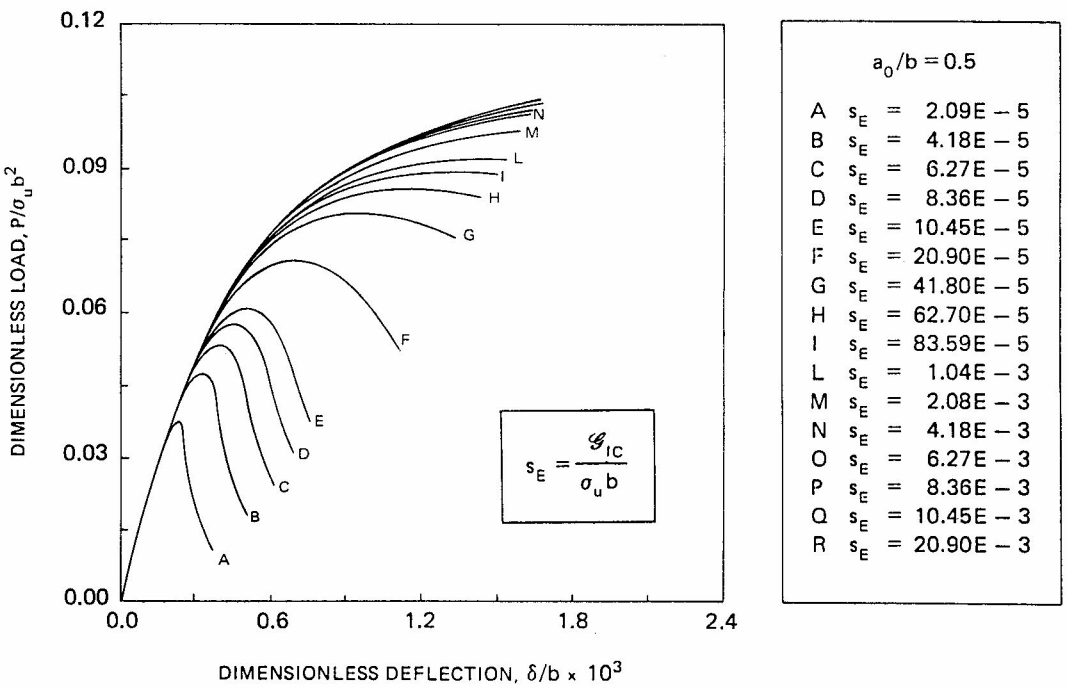

Fig. 8(c)

Fig. 8. Dimensionless load–deflection diagrams by varying the brittleness number s_E: (a) $a_0/b = 0.1$; (b) $a_0/b = 0.3$: (c) $a_0/b = 0.5$.

load $P^{(2)}_{max}$ according to LEFM can be derived from eq. (2). The values of the ratio $P^{(1)}_{max}/P^{(2)}_{max}$ are reported as functions of the inverse of the brittleness number, s_E, in Fig. 9. The ratio $P^{(1)}_{max}/P^{(2)}_{max}$ may also be regarded as the ratio of the fictitious fracture toughness (given by the maximum load $P^{(1)}_{max}$) to the true fracture toughness (considered as a material constant).

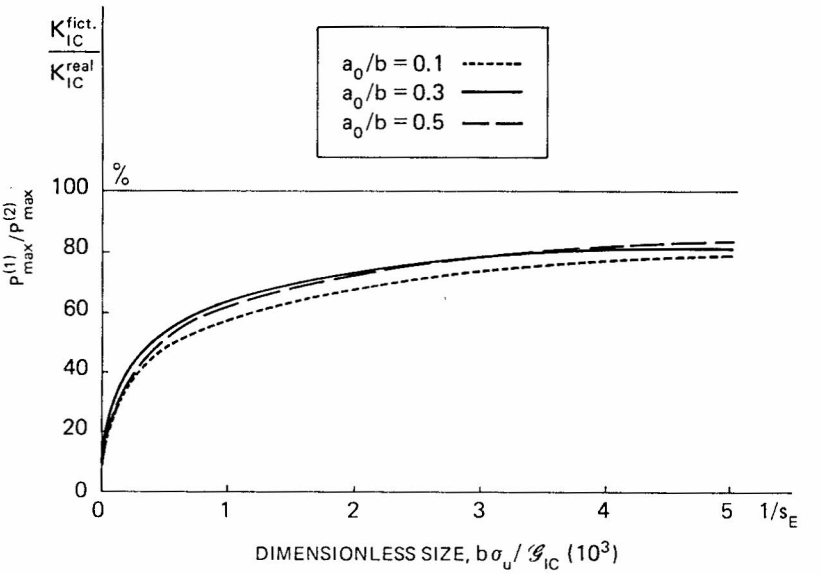

Fig. 9. Size-scale transition towards LEFM.

It is evident that, for low s_E values, the results of the cohesive crack model tend to those of LEFM [10]:

$$\lim_{s_E \to 0} P_{max}^{(1)} = P_{max}^{(2)}, \tag{25}$$

and, therefore, the maximum loading capacity can be predicted by applying the simple condition $K_I = K_{IC}$.

The fictitious crack depth at the maximum load is plotted as a function of the inverse of brittleness number, s_E, in Fig. 10. The brittleness increase for $s_E \to 0$ is evident also from these diagrams: the process zone at $dP/d\delta = 0$ tending to disappear (brittle fracture), whereas it tends to cover the whole ligament for $s_E \to \infty$ (ductile collapse). The real (or stress-free) crack depth at the maximum load is nearly coincident with the initial crack depth for each value of s_E. This means that the slow crack growth does not start before the softening stage. Therefore, neither the slow crack growth occurs nor the cohesive zone develops before the peak, when $s_E \to 0$.†

Recalling once again Figs 9 and 10, it is possible to state that, the smaller the brittleness number, s_E, is, i.e. the lower the fracture toughness, $\mathcal{G}_{IC}$, the larger the size-scale b and/or the higher the ultimate tensile strength σ_u, and the more accurate the cusp catastrophe is in reproducing the classical LEFM instability [10–12].

6. ENERGY DISSIPATION IN THE FRACTURING PROCESS

If the loading process is controlled by a monotonically increasing function of time, like, for instance, the crack mouth opening displacement [4] or the linear combination of load and displacement ($\delta \cos\theta - P \sin\theta$), where θ represents a rotation of the control plane δ versus P about the origin [13], the snap-back behaviour in the load–displacement curve can be captured experimentally. When the post-peak behaviour is kept under control up to the complete structure separation, the area delimited by load–displacement curve and displacement axis represents the product of strain energy release rate, $\mathcal{G}_{IC}$, by the initial ligament area, $(b - a_0)t$. The areas under the $P - \delta$ curves in Fig. 8 are thus proportional to the respective s_E numbers. This simple result is due to the assumption that energy dissipation occurs only on the fracture surface, whereas in reality energy is also dissipated in a damage volume around the crack tip, as is assumed by Carpinteri and Sih in [14] and by Carpinteri in [15].

†Slow crack growth and cohesive zone may develop only if both load and displacement are decreased, following the virtual branch with positive slope. On the other hand, with normal softening (i.e. only negative slope in the P–δ curve after the peak), only the load must be decreased to control the fracture process.

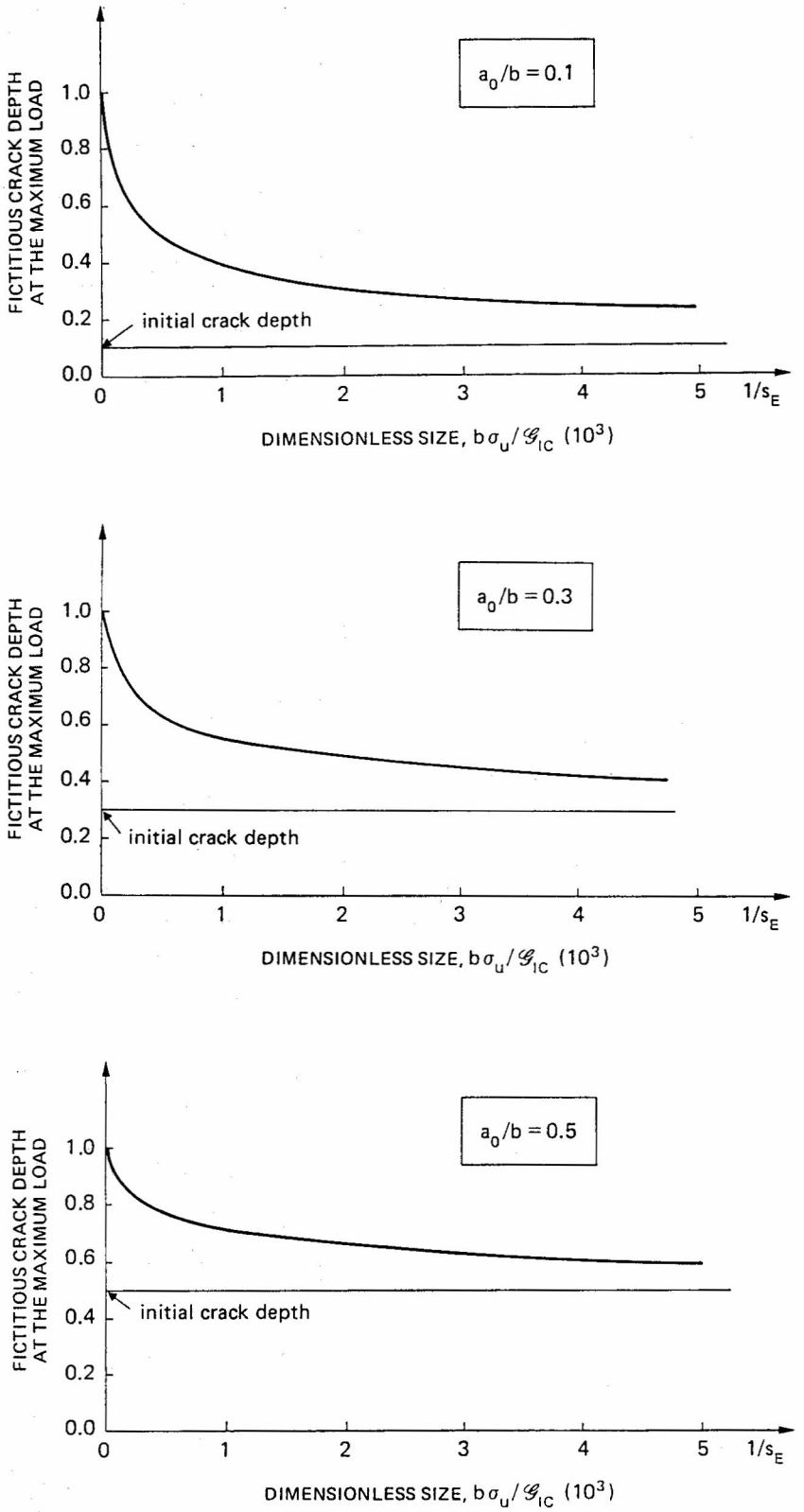

Fig. 10. Fictitious crack depth at the maximum load as a function of dimensionless size. (a) $a_0/b = 0.1$; (b) $a_0/b = 0.3$; (c) $a_0/b = 0.5$.

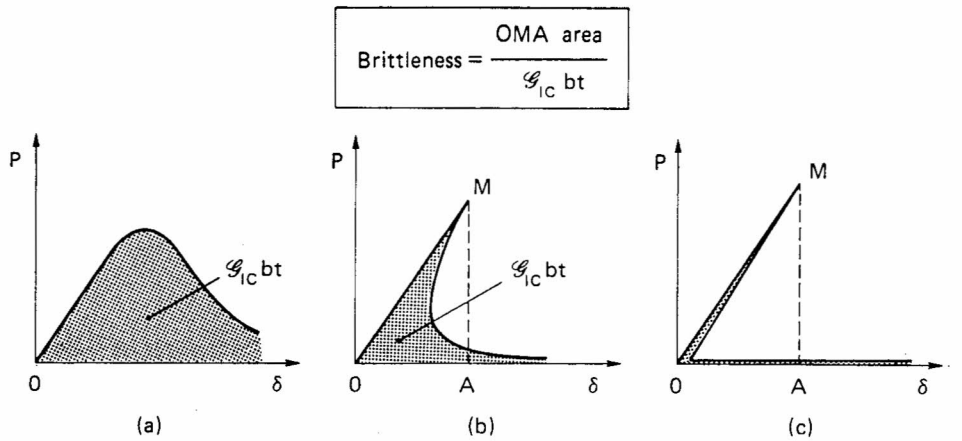

Fig. 11. Load–deflection diagrams for an initially uncracked beam ($a_0 = 0$): small (a), intermediate (b) and large (c) size.

When the brittleness number $s_E \to 0$, $P^{(1)}_{max} \simeq P^{(2)}_{max}$ and eqs (2) and (23) provide:

$$\mathcal{G}_{IC} = P^2_{max} \frac{(l/b)^2 f^2(a_0/b)}{bt^2 E}. \tag{26}$$

On the other hand, since the deflection is given by eq. (9), which is valid also at the maximum load, eq. (26) is transformed as follows:

$$\mathcal{G}_{IC}(b - a_0)t = (P_{max}\delta_{max}/2) \frac{2f^2\left(\frac{a_0}{b}\right)\left(1 - \frac{a_0}{b}\right)}{\frac{1}{4}\left(\frac{l}{b}\right) + \frac{3}{2}g\left(\frac{a_0}{b}\right)}. \tag{27}$$

If *brittleness* is defined as the ratio of the elastic energy contained in the body at the maximum load to the energy which can be dissipated in the body, it proves to be a function of beam slenderness and initial crack depth (Fig. 11a, b):

$$\begin{aligned} brittleness &= \frac{\frac{1}{2}P_{max}\delta_{max}}{\mathcal{G}_{IC}(b - a_0)t} \\ &= \frac{\frac{1}{4}\left(\frac{l}{b}\right) + \frac{3}{2}g\left(\frac{a_0}{b}\right)}{2\left(1 - \frac{a_0}{b}\right)f^2\left(\frac{a_0}{b}\right)}. \end{aligned} \tag{28}$$

When the beam is initially uncracked, i.e. $a_0/b = 0$, the brittleness tends to infinity and the softening branch is coincident with the elastic one (Fig. 11c). On the other hand, when the initial crack length is different from zero, i.e. $a_0 \neq 0$, the brittleness tends to the finite value in eq. (28) for the size-scale tending to infinite. In this case, the softening branch is always distinct from the elastic one.

When the beam is initially uncracked, the elastic energy contained in the body at the point of instability is an infinite quantity of higher rank with respect to the fracture energy; the former being proportional to $b^3(\sigma_u^2/E)$ and the latter to $b^2\mathcal{G}_{IC}$. When there is an initial crack, the two quantities are of the same rank for the size-scale b tending to infinity, their ratio being finite and provided in eq. (28).

Acknowledgements—The numerical results reported in the present paper were obtained in a joint research program between ENEL-CRIS-Milano and the University of Bologna. The Department of Public Education (M.P.I.) is acknowledged for the financial support provided to the present research.

REFERENCES

[1] A. Carpinteri, Size effect in fracture toughness testing: a dimensional analysis approach. *Proc. Int. Conf. Analytical and Experimental Fracture Mechanics*, Roma (23–27 June, 1980) (Edited by G. C. Sih and M. Mirabile), pp. 785–797. Sijthoff & Noordhoff, The Netherlands (1981).
[2] A. Carpinteri, Notch sensitivity in fracture testing of aggregative materials. *Engng Fracture Mech.* **16,** 467–481 (1982).
[3] A. Carpinteri, C. Marega and A. Savadori, Ductile–brittle transition by varying structural size. *Engng Fracture Mech.* **21,** 263–271 (1985).
[4] L. Biolzi, S. Cangiano, G. Tognon and A. Carpinteri, Snap-back softening instability in high strength concrete beams. *SEM/RILEM Int. Conf. Fracture of Concrete and Rock*, Houston, Texas (17–19 June, 1987).
[5] *Standard Method of Test for Plane Strain Fracture Toughness of Metallic Materials*, E 399–74, ASTM.
[6] H. Tada, P. Paris and G. Irwin, *The Stress Analysis of Cracks Handbook*, pp. 2.16–17. Del Research Corporation, St. Louis, Missouri (1963).
[7] J. P. Berry, Some kinetic considerations of the Griffith criterion for fracture. *J. Mech. Phys. Solids* **8,** 194–216 (1960).
[8] A. Hillerborg, M. Modeer and P. E. Petersson, Analysis of crack formation and crack growth in concrete by means of fracture mechanics and finite elements. *Cement Concr. Res.* **6,** 773–782 (1976).
[9] P. E. Petersson, Crack growth and development of fracture zones in plane concrete and similar materials. Report TVBM-1006, Division of Building Materials, Lund Institute of Technology (1981).
[10] A. Carpinteri, Interpretation of the Griffith instability as a bifurcation of the global equilibrium. *Application of Fracture Mechanics to Cementitious Composites, NATO Advanced Research Workshop*. Northwestern University (4–7 September, 1984); (Edited by S. P. Shah), pp. 287–316. Martinus Nijhoff, The Hague (1985).
[11] A. Carpinteri and M. Fanelli, Numerical analysis of the catastrophical softening behaviour in brittle structures. *4th Int. Conf. on Numerical Methods in Fracture Mechanics*, San Antonio, Texas (23–27 March, 1987), pp. 369–386. Pineridge Press, Swansea.
[12] A. Carpinteri, A catastrophe theory approach to fracture mechanics. *Int. Conf. Role of Fracture Mechanics in Modern Technology*, Fukuoka (Japan) (2–6 June, 1986).
[13] K. Rokugo, S. Ohno and W. Koyanagy, Automatical measuring system of load–displacement curves including post-failure region of concrete specimen. *Int. RILEM Conf. Fracture Mechanics of Concrete*, Lausanne (1–3 October, 1985) Switzerland (Edited by F. H. Wittmann), pp. 403–411. Elsevier.
[14] A Carpinteri and G. C. Sih, Damage accumulation and crack growth in bilinear materials with softening. *Theor. appl. Fracture Mech.* **1,** 145–160 (1984).
[15] A. Carpinteri, *Mechanical Damage and Crack Growth in Concrete*. Martinus Nijhoff, The Hague (1986).

(*Received* 30 *December* 1987)